Article
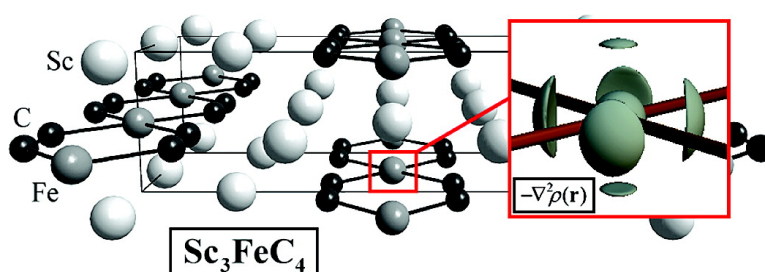
Experimental Electron Density of the Complex Carbides Sc[Fe(C)] and Sc[Co(C)]

Benjamin Rohrmoser, Georg Eickerling, Manuel Presnitz, Wolfgang Scherer, Volker Eyert, Rolf-Dieter Hoffmann, Ute Ch. Rodewald, Christian Vogt, and Rainer Pttgen

More About This Article

Additional resources and features associated with this article are available within the HTML version:

- Supporting Information
- Links to the 7 articles that cite this article, as of the time of this article download
- Access to high resolution figures
- Links to articles and content related to this article
- Copyright permission to reproduce figures and/or text from this article

View the Full Text HTML

Experimental Electron Density of the Complex Carbides Sc$_3$[Fe(C$_2$)$_2$] and Sc$_3$[Co(C$_2$)$_2$]

Benjamin Rohrmoser,[†] Georg Eickerling,[†] Manuel Presnitz,[†] Wolfgang Scherer,*,[†] Volker Eyert,*,[†] Rolf-Dieter Hoffmann,[‡] Ute Ch. Rodewald,[‡] Christian Vogt,[‡] and Rainer Pöttgen*,[‡]

Contribution from the Institut für Physik, Universität Augsburg, Universitätsstrasse 1, 86159 Augsburg, Germany, and Institut für Anorganische und Analytische Chemie, Westfälische Wilhelms-Universität Münster, Corrensstrasse 30, 48149 Münster, Germany

Received November 14, 2006; E-mail: wolfgang.scherer@physik.uni-augsburg.de; volker.eyert@physik.uni-augsburg.de; pottgen@uni-muenster.de

Abstract: The nature of chemical bonding in the complex carbides Sc$_3$[Fe(C$_2$)$_2$] (**1**) and Sc$_3$[Co(C$_2$)$_2$] (**2**) has been explored by combined experimental and theoretical charge density studies. The structures of these organometallic carbides contain one-dimensional infinite TC$_4$ (T = Fe, Co) ribbons embedded in a scandium matrix. Bonding in **1** and **2** was studied experimentally by multipolar refinements based on high-resolution X-ray data and compared to scalar-relativistic electronic structure calculations using the augmented spherical wave method. Besides substantial covalent T−C bonding within the TC$_4$ ribbons, one also observes discrete Sc−C bonds of noticeable covalent character. Furthermore, our study highlights that even tiny differences in the electronic band structure of solids might be faithfully recovered in the properties of the Laplacian of the experimental electron density. In our case, the increase of the Fermi level in the organometallic Co(d^9) carbide **2** relative to its isotypic Fe(d^8) species **1** is reflected in the charge density picture by a significant change in the polarization pattern displayed by valence shell charge concentrations of the transition metal centers in the TC$_4$ units. Hence, precise high-resolution X-ray diffraction data provide a reliable tool to discriminate and analyze the local electronic structures of isotypic solids, even in the presence of a severe coloring problem (Z(Fe)/Z(Co) = 26/27).

1. Introduction

Complex carbides of the rare earth (*RE*) and transition (*T*) metals exhibit an enormous structural variety and interesting magnetic and electrical properties. The many $RE_xT_yC_z$ carbides have been investigated intensively by the groups of Jeitschko and Bodak.[1−3] Dominant structural features of these carbides are zero-, one-, two-, or three-dimensional [T_yC_z] polyanions

that resemble the organometallic motifs in metal carbonyls. In the case of zero-, one-, and two-dimensional polyanions, the [T_yC_z] units are embedded in the rare earth metal matrix, while the rare earth metal atoms are located in cages or channels when the polyanions are three-dimensional. Many of the polyanions contain C$_2$ pairs with C−C distances spanning a wide range from 1.27 to 1.48 Å,[4] indicating different bond orders. Cutouts of the organometallic polyanions in CeRhC$_2$,[5] SmRhC$_2$,[5] Sc$_3$-RuC$_4$,[6] UCoC$_2$,[7] Yb$_4$Ni$_2$C$_5$,[8] and Er$_2$MnC$_4$[9] are presented in Figure 1.

Many of the $RE_xT_yC_z$ carbides have been studied with respect to their magnetic and conductivity behavior. Recent interesting examples are the semiconductors LaRhC$_2$ and CeRhC$_2$,[5] the 3.6

[†] Universität Augsburg.
[‡] Westfälische Wilhelms-Universität Münster.
(1) (a) Bodak, O. I.; Marusin, E. P. *Dokl. Akad. Nauk Ukr. SSR Ser. A* **1979**, *12*, 1048−1050. (b) Bodak, O. I.; Marusin, E. P.; Bruskov, V. A. *Kristallografiya* **1980**, *25*, 617−619. (c) Tsokol', A. O.; Bodak, O. I.; Marusin, E. P. *Kristallografiya* **1986**, *31*, 788−790. (d) Tsokol', A. O.; Bodak, O. I.; Marusin, E. P.; Zavodnik, V. E. *Kristallografiya* **1988**, *33*, 345−348. (e) Pecharskaya, A. O.; Marusin, E. P.; Bodak, O. I.; Mazus, M. D. *Kristallografiya* **1990**, *35*, 47−49.
(2) (a) Pöttgen, R.; Witte, A. M.; Jeitschko, W.; Ebel, T. *J. Solid State Chem.* **1995**, *119*, 324−330. (b) Reehuis, M.; Danebrock, M. E.; Rodriguez-Carvajal, J.; Jeitschko, W.; Stüsser, N.; Hoffmann, R.-D. *J. Magn. Magn. Mater.* **1996**, *154*, 355−364. (c) Böcker, U. A.; Jeitschko, W.; Block, G. *J. Alloys Compd.* **1996**, *236*, 58−62. (d) Pöttgen, R.; Wachtmann, K. H.; Jeitschko, W.; Lang, A.; Ebel, T. *Z. Naturforsch.* **1997**, *52b*, 231−236. (e) Hoffmann, R.-D.; Jeitschko, W. *Acta Crystallogr.* **1998**, *B54*, 834−850. (f) Hüfken, Th.; Wachtmann, K. H.; Jeitschko, W. *J. Alloys Compd.* **1998**, *281*, 233−236. (g) Reehuis, M.; Gerdes, M.; Jeitschko, W.; Ouladdiaf, B.; Stüsser, N. *J. Magn. Magn. Mater.* **1999**, *195*, 657−666. (h) Pohlkamp, M. W.; Hoffmann, R.-D.; Kotzyba, G.; Jeitschko, W. *J. Solid State Chem.* **2001**, *160*, 77−87. (i) Pohlkamp, M. W.; Kotzyba, G.; Böcker, U. A.; Gerdes, M. H.; Wachtmann, K. H.; Jeitschko, W. *Z. Anorg. Allg. Chem.* **2001**, *627*, 341−348.

(3) Adachi, G.-Y.; Imanaka, N.; Fuzhong, Zh. Rare Earth Carbides. In *Handbook on the Physics and Chemistry of Rare Earths*; Gschneidner, K. A., Jr., Eyring, L., Eds.; North Holland: Amsterdam, 1991; Chapter 99, pp 61−190.
(4) Jeitschko, W.; Gerss, M. H.; Hoffmann, R.-D.; Lee, St. *J. Less-Common Met.* **1989**, *156*, 397−412.
(5) Hoffmann, R.-D.; Jeitschko, W.; Boonk, L. *Chem. Mater.* **1989**, *1*, 580−586.
(6) Hoffmann, R.-D.; Pöttgen, R.; Jeitschko, W. *J. Solid State Chem.* **1992**, *99*, 134−139.
(7) Gerss, M. H.; Jeitschko, W. *Mater. Res. Bull.* **1986**, *21*, 209−216.
(8) Musanke, U. E.; Jeitschko, W.; Danebrock, M. E. *Z. Anorg. Allg. Chem.* **1992**, *619*, 321−326.
(9) Kahnert, G. E.; Jeitschko, W.; Block, G. *Z. Anorg. Allg. Chem.* **1993**, *619*, 442−446.
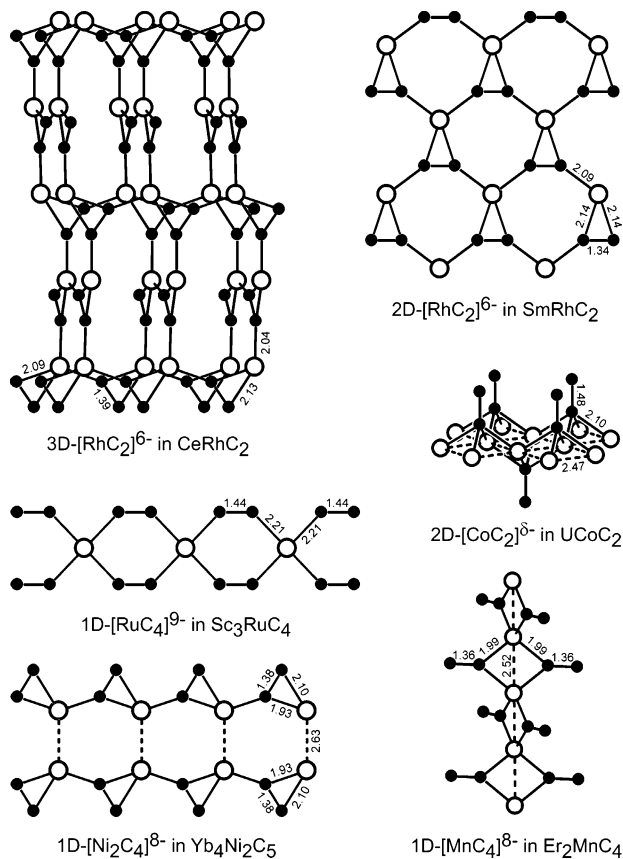
Figure 1. Cutouts of the transition metal−carbon polyanions in the structures of CeRhC$_2$, SmRhC$_2$, Sc$_3$RuC$_4$, UCoC$_2$, Yb$_4$Ni$_2$C$_5$, and Er$_2$MnC$_4$. All distances are given in Ångströms.

K superconductor Y$_2$FeC$_4$,[10] the superconducting solid solution La$_{1-x}$Th$_x$NiC$_2$,[11] and the ferromagnets Gd$_2$OsC$_2$ and Tb$_2$OsC$_2$[12] with comparatively high Curie temperatures of 320 and 210 K, respectively. YCoC has a relatively high electronic specific heat coefficient of $\gamma = 14$ mJ/(K^2·mol), suggesting narrow conduction bands.[13]

Chemical bonding in the $RE_xT_yC_z$ carbides can, to a first approximation, be rationalized by simple electron counting,[2,8,9,14−16] assuming that the electropositive rare earth metal atoms have transferred their valence electrons to the transition metal and carbon atoms, enabling the covalent T−C and C−C bonding. These considerations readily showed that the transition metal atoms mostly obey the 18-electron rule. Extended Hückel electronic structure calculations by the Hoffmann group[17−21] underlined this view of chemical bonding.

We have now started first studies on the experimental electron density of the scandium-containing carbides via high-angle single-crystal diffractometry and ^{13}C solid-state NMR spectroscopy. The Sc$_3$TC$_4$ carbides exist with Mn, Fe, Co, Ni, Ru, Rh, Os, and Ir as transition metal component.[1c,6,22,23] While room-temperature single-crystal data of Sc$_3$FeC$_4$ and Sc$_3$RuC$_4$ reveal the undistorted Sc$_3$CoC$_4$-type structure, different superstructures have been observed for Sc$_3$RhC$_4$ and Sc$_3$IrC$_4$ at ambient temperature[23] and for Sc$_3$RuC$_4$ and Sc$_3$OsC$_4$ at low temperature.[24] These superstructures are due to different puckering effects.

Herein, we report on the first experimental electron density study on Sc$_3$FeC$_4$ and Sc$_3$CoC$_4$, and we compare the experimental data with theoretical data derived from electronic structure calculations.

2. Experimental Section

Synthesis and Characterization. Starting materials for the synthesis of Sc$_3$FeC$_4$ and Sc$_3$CoC$_4$ were scandium filings (Kelpin), iron powder (325 mesh, Ventron), cobalt powder (100 mesh, Aldrich), and graphite flakes (10 mesh, Alfa Aesar), all with stated purities better than 99.9%. The elements were mixed in the atomic ratio 3:1:4, cold-pressed into pellets (6 mm diameter), and arc-melted[25] under an argon atmosphere of ca. 600 mbar. The argon was purified, before use, over titanium sponge (870 K), silica gel, and molecular sieves. Each sample was remelted three times from both sides to ensure homogeneity. The total weight loss after the melting procedures was smaller than 2 wt %. Sc$_3$FeC$_4$ and Sc$_3$CoC$_4$ are stable in air over months. For crystal growth, the arc-melted sample was sealed in an evacuated silica ampule and annealed for 4−6 h slightly below the (undetermined) melting point in a special water-cooled sample chamber in an induction furnace (Hüttinger TIG 5/300).[26] For further details, we refer the reader to the previous work.[6]

X-ray Data Collection. The samples were characterized through Guinier powder patterns using Cu $K\alpha_1$ radiation and α-quartz ($a = 4.9130$, $c = 5.4046$ Å) as an internal standard. The Guinier camera was equipped with an image plate system (Fujifilm, BAS-1800). The indexing of the powder patterns was facilitated by intensity calculations[27] using the positional parameters from the present structure refinements: Sc$_3$FeC$_4$ [Sc$_3$CoC$_4$], $a = 3.3698(5)$ [3.3956(5)], $b = 4.3822(8)$ [4.3739(7)], and $c = 12.101(2)$ [11.989(2)] Å, $V = 178.7(1)$ [178.1(1)] Å^3. The lattice parameters derived from the crystalline powders agree well with those obtained from the single crystals. A gray needle type [cuboid] crystal of Sc$_3$FeC$_4$ [Sc$_3$CoC$_4$] with the dimensions $0.020 \times 0.030 \times 0.120$ [$0.020 \times 0.045 \times 0.090$] mm was selected from the crushed, annealed samples, glued to quartz fibers using a transparent varnish, and then examined on a Buerger precession camera (equipped with the same image plate system) with white Mo radiation in order to control its quality and lattice parameters. Final data collections were carried out with graphite-monochromated Mo $K\alpha$ radiation ($\lambda = 0.71073$ Å) at room temperature on an automated four-circle diffractometer (CAD4) equipped with a scintillation counter with pulse-height discrimination.

X-ray Data Reduction. Crystal data for Sc$_3$FeC$_4$ [Sc$_3$CoC$_4$]: $M_r = 238.76$ [241.85], orthorhombic [orthorhombic], space group *Immm*

(10) Gerss, M. H.; Jeitschko, W.; Boonk, L.; Nientiedt, J.; Grobe, J.; Mörsen, E.; Leson, A. *J. Solid State Chem.* **1987**, *70*, 19−28.
(11) (a) Lee, W. H.; Zheng, H. K. *Solid State Commun.* **1997**, *101*, 323−326. (b) Lee, W. H.; Zheng, H. K.; Chen, Y. Y.; Yao, Y. D.; Ho, J. C. *Solid State Commun.* **1997**, *102*, 433−436.
(12) Gerdes, M. H.; Jeitschko, W.; Wachtmann, K. H.; Danebrock, M. E. *J. Mater. Chem.* **1997**, *7*, 2427−2431.
(13) Suzuki, K.; Murayama, T.; Eguchi, M. *J. Alloys Compd.* **2001**, *317−318*, 306−310.
(14) King, R. B. *Russ. Chem. Bull.* **1994**, *43*, 1285−1292.
(15) King, R. B. *J. Organomet. Chem.* **1997**, *536/537*, 7−15.
(16) King, R. B. *J. Ind. Chem. Soc.* **2000**, *77*, 603−607.
(17) Hoffmann, R.; Li, J.; Wheeler, R. A. *J. Am. Chem. Soc.* **1987**, *109*, 6600−6602.
(18) Li, J.; Hoffmann, R. *Chem. Mater.* **1989**, *1*, 83−101.
(19) Deng, H.; Hoffmann, R. *Inorg. Chem.* **1993**, *32*, 1991−1996.
(20) Merschrod, E. F.; Tang, S. H.; Hoffmann, R. *Z. Naturforsch.* **1998**, *53b*, 322−332.
(21) Merschrod, E. F.; Courtney, A.; Hoffmann, R. *Z. Anorg. Allg. Chem.* **2002**, *628*, 2757−2763.

(22) Wachtmann, K. Strukturchemische Untersuchungen ternärer Seltenerdmetall- und Actinoid-Carbide mit Haupt- und Nebengruppenelementen. Dissertation, Universität Münster, 1995.
(23) Vogt, C.; Hoffmann, R.-D.; Pöttgen, R. *Solid State Sci.* **2005**, *7*, 1003−1009.
(24) Vogt, C.; Hoffmann, R.-D.; Rodewald, U. Ch.; Pöttgen, R.; Rohrmoser, B.; Scherer, W. *Z. Anorg. Allg. Chem.* **2006**, *632*, 2116.
(25) Pöttgen, R.; Gulden, Th.; Simon, A. *GIT Labor-Fachzeitschrift* **1999**, *43*, 133−136.
(26) Niepmann, D.; Prots', Yu. M.; Pöttgen, R.; Jeitschko, W. *J. Solid State Chem.* **2000**, *154*, 329−337.
(27) Yvon, K.; Jeitschko, W.; Parthé, E. *J. Appl. Crystallogr.* **1977**, *10*, 73−74.

[*Immm*], $a = 3.3689(10)$ [3.3935(10)], $b = 4.3818(10)$ [4.3687(10)], and $c = 12.0959(10)$ [11.9851(10)] Å, $V = 178.56(7)$ [177.68(7)] Å^3; $T = 293(2)$ [293(2)] K; $Z = 2$ [2], $F(000) = 226$ [228], $D_{calc} = 4.441$ [4.521] g/cm^3, $\mu = 9.20$ [9.83] mm^{-1}. A numerical absorption correction was then applied ($T_{min} = 0.682$, $T_{max} = 0.862$ [$T_{min} = 0.579$, $T_{max} = 0.780$]) with the programs X-RED and X-SHAPE[28] using a data set of 700 equivalent and 110 unique reflections [1427 equivalent, 282 unique reflections] extracted from the collected data set. The internal agreement factor was $R_{int}(F) = 0.0578$ [0.0312] for a total of 6787 [6755] reflections yielding 1018 [1013] unique reflections. This data set provided 100% of data in $2 < 2\theta < 140°$ (sin $\theta/\lambda < 1.322$ Å^{-1}).

Multipolar Refinements and Determination of the Deformation Density. First, an independent atom model (IAM) refinement was carried out, in which all atoms were treated as spherical. Anisotropic displacement parameters were introduced to describe the thermal motion of all atoms. The refinement finally converged at $R_1 = 0.0271$ [0.0193], $wR_2 = 0.0391$ [0.0321], and GOF $= 1.052$ [1.075] for all reflections and 18 [18] parameters.[29] A multipole model was then adopted to describe the deformation of $\rho(\mathbf{r})$ from a spherical distribution. According to a method proposed by Stewart,[30] the electron density $\rho(\mathbf{r})$ in a crystal is described by a sum of aspherical pseudoatoms at the nuclear positions $\{\mathbf{R}_j\}$:

$$\rho(\mathbf{r}) = \sum_j \rho_j(\mathbf{r} - \mathbf{R}_j)$$

Based on the Hansen–Coppens formalism,[31] the pseudoatom density ρ_{at} is expressed in terms of multipoles:[32]

$$\rho_{at}(\mathbf{r}) = P_c\rho_{core}(\mathbf{r}) + P_v\kappa^3\rho_{valence}(\kappa\mathbf{r}) +$$
$$\sum_{l=0}^{l_{max}} \kappa'^3 R_l(\kappa'\mathbf{r}) \sum_{m=0}^{l} P_{lm\pm}d_{lm\pm}(\theta,\phi)$$

In the refinement of our best model, the multipole expansion was truncated at the hexadecapole level ($l_{max} = 4$ [$l_{max} = 4$]) for all atoms. Core and spherical valence densities were constructed using wave functions fitted to a relativistic Dirac–Fock solution,[33] which were then expanded over Slater-type basis functions. Single-ζ functions are taken from Clementi and Raimondi and were used to model the radial distribution of the deformation density.[34]

At the beginning of the multipolar refinements, the atomic coordinates and displacement parameters were fixed at the values obtained by a preceding high-order refinement (sin $\theta/\lambda > 0.8$ Å^{-1} [sin $\theta/\lambda > 0.8$ Å^{-1}]). In a final refinement step, however, the coordinates and atomic displacement parameters were allowed to relax and were optimized along with all multipolar parameters of our final model.

Individual radial scaling parameters (κ), to adjust the spherical atomic density contributions, were refined for each crystallographically independent atom present in the asymmetric unit (four in total). In addition, a radial scaling parameter (κ') was assigned, one for each individual element of the ternary carbides (three in total). The κ for both Sc atoms and κ' values for the Sc and C atoms were fixed during the refinements to reach convergency of the models. The total charge of the asymmetric unit was constrained to zero during all refinements. The final agreement factors were $R_1 = 0.0155$ [0.0122], $wR_2 = 0.0264$ [0.0160], and GOF $= 1.1083$ [1.1971] for 853 [910] reflections ($F_o >$

$3\sigma(F_o)$) and 55 [55] parameters ($N_{ref}/N_{var} = 15.5$ [16.5]); see S2 and S3 in the Supporting Information for final multipole population parameters and fractional atomic coordinates.

All refinements were carried out with the full-matrix least-squares program XDLSM of the XD suite of programs;[32] the quantity minimized was $\epsilon = \sum w_1(|F_o| - k|F_c|)^2$, where k is a scale factor, based on 853 [910] reflections with $F_o > 3\sigma(F_o)$. Weights were taken as $w_1 = 1/\sigma^2(F_o)$ and $w_2 = 1/\sigma^2(F_o^2)$. Convergence was assumed when a maximal shift/esd $< 10^{-11}$ was achieved. The residual electron density maps were practically featureless, with the maximum and minimum values of 0.283 [0.286] and -0.357 [-0.246] e/Å^3 (sin $\theta/\lambda < 0.8$ Å^{-1} [sin $\theta/\lambda < 0.8$ Å^{-1}]), respectively. For the topological analysis, critical points of the electron density were searched via a Newton–Raphson algorithm implemented in TOPXD[35] or alternatively by using the XDPROP module of the XD suite of programs. Properties of $\rho(\mathbf{r})$ and $\nabla^2\rho(\mathbf{r})$ were calculated after transformation of the local axis system into a global system.

Computational Details. The calculations were performed using the scalar-relativistic augmented spherical wave (ASW) method.[36,37] Here, we used a new version of the ASW code, which takes into account the non-spherical contributions to the charge density and the potential inside the atomic spheres.[38] In the ASW method, the wave function is expanded in atom-centered augmented spherical waves, which are Hankel functions and numerical solutions of Schrödinger's equation, respectively, outside and inside the so-called augmentation spheres. In order to optimize the basis set, additional augmented spherical waves were placed at carefully selected interstitial sites. The choice of these sites as well as the augmentation radii were automatically determined using the sphere-geometry optimization (SGO) algorithm.[39] Both the local density approximation (LDA) and the generalized gradient approximation (GGA)[40] were used. Self-consistency was achieved by using a highly efficient algorithm for convergence acceleration.[41] The Brillouin zone sampling was done using an increased number of up to 512 **k**-points in the irreducible wedge of the body-centered orthorhombic Brillouin zone. For the comparison of the topology of the experimental and theoretical charge density distributions in **1** and **2**, the WIEN2K program was employed.[42] The calculated charge densities were obtained using the gradient-corrected density functional of Perdew, Burke, and Ernzerhoff (PBE)[43] and an augmented plane wave basis set with additional local orbitals (APW+lo). We used the geometry and crystallographic parameters of our final multipolar refinements without any further geometry optimization as the input model for the SCF calculations. Scalar fields of the negative Laplacian, $L(\mathbf{r}) = -\nabla^2\rho(\mathbf{r})$, were obtained using the LAPW0 routine of the WIEN2K code. The identification, localization, and magnitude of the local charge concentrations were obtained numerically using the XCRYSDEN code.[44] The topological parameters at the critical points of the $\rho(\mathbf{r})$ distribution in the framework of Bader's quantum theory of atoms in molecules (QTAM)[45] were obtained using the implemented atoms in molecules (AIM) routines of the WIEN2K code. Atomic charges were computed via integration of $\rho(\mathbf{r})$ over the individual atomic basins of **1** and **2**.

(28) *X-RED32*, Version 1.10; *X-SHAPE*, Version 2.05; program package for crystal shape refinement; STOE & Cie GmbH: Darmstadt, Germany, 2004.
(29) Sheldrick, G. M. *SHELXL-97*, program for crystal structure refinement; University of Göttingen: Göttingen, Germany 1997.
(30) Stewart, R. F. *Acta Crystallogr.* **1976**, *A32*, 565−574.
(31) Hansen, H. K.; Coppens, P. *Acta Crystallogr.* **1978**, *A34*, 909−921.
(32) Koritsanszky, T.; Howard, S. T.; Su, Z.; Mallinson, P. R.; Richter, T.; Hansen, N. K. *XD*, Revision 4.10, Computer Program Package for Multipole Refinement and Analysis of Electron Densities from Diffraction Data; Free University of Berlin: Berlin, Germany, July 2003.
(33) Su, Z.; Coppens, P. *Acta Crystallogr.* **1998**, *A54*, 646−652.
(34) Clementi, E.; Raimondi, D. L. *J. Chem. Phys.* **1963**, *38*, 2686−2689.

(35) Volkov, A.; Gatti, C.; Abramov, Y.; Coppens, P. *Acta Crystallogr.* **2000**, *A56*, 252−258.
(36) Williams, A. R.; Kübler, J.; Gelatt, C. D., Jr. *Phys. Rev. B* **1979**, *19*, 6094−6118.
(37) Eyert, V. *Int. J. Quantum Chem.* **2000**, *77*, 1007−1031.
(38) Eyert, V. *The Augmented Spherical Wave Method−A Comprehensive Treatment*; Lecture Notes in Physics 719; Springer: Heidelberg, 2007.
(39) Eyert, V.; Höck, K.-H. *Phys. Rev. B* **1998**, *57*, 12727−12737.
(40) Wu, Z.; Cohen, R. E. *Phys. Rev. B* **2006**, *73*, 235116(6).
(41) Eyert, V. *J. Comput. Phys.* **1996**, *124*, 271−285.
(42) Schwarz, K.; Blaha, P.; Madsen, G.; Kvasnicka, D.; Luitz, J. *WIEN2K*, An Augmented Plane Wave + Local Orbitals Program for Calculating Crystal Properties: Technische Universität Wien: Vienna, Austria, 2003.
(43) (a) Perdew, J. P.; Burke, K.; Ernzerhoff, M. *Phys. Rev. Lett.* **1996**, *77*, 3865−3868. (b) Perdew, J. P.; Burke, K.; Ernzerhoff, M. *Phys. Rev. Lett.* **1997**, *78*, 1396.
(44) Kokalj, A. *Comput. Mater. Sci.* **2003**, *28*, 155−168.
(45) Bader, R. F. W. *Atoms in Molecules−A Quantum Theory*; Oxford University Press: Oxford, U.K., 1994.
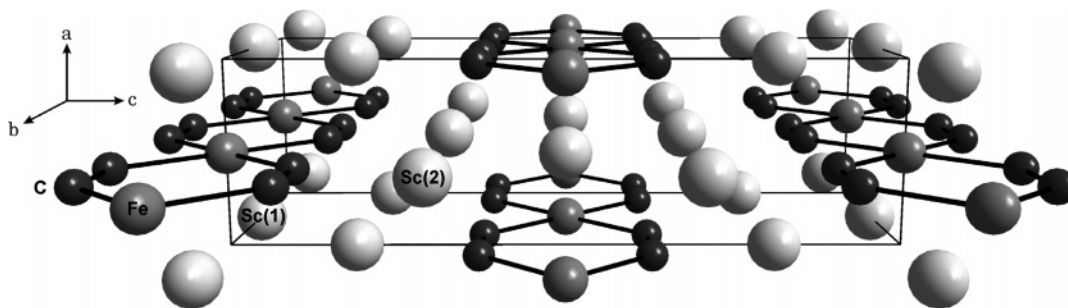
Figure 2. View of the Sc_3FeC_4 structure approximately along the [010] direction. The scandium, iron, and carbon atoms are drawn as medium gray, gray, and black circles, respectively. The one-dimensional $[FeC_4]^{9-}$ polyanionic chains are emphasized.

3. Results and Discussion

Crystal Chemistry. A view of the Sc_3FeC_4 structure approximately along the crystallographic *b*-axis is presented in Figure 2. The one-dimensional $[FeC_4]^{9-}$ polyanions extend along the *b*-axis and are embedded in the scandium matrix. Within the $[FeC_4]^{9-}$ polyanion, each iron atom is coordinated by four C_2 pairs at Fe$-$C distances of 2.1074(6) Å, slightly longer than the sum of the covalent radii for iron and carbon of 1.94 Å.[46] The C_2 pairs display a C$-$C distance of 1.450(1) Å, suggesting an intermediate bonding situation between a C$-$C single bond (1.54 Å) and a double bond (1.34 Å).

Due to the high scandium content, we observe a variety of Sc$-$Sc contacts, with Sc$-$Sc distances ranging from 3.17 to 3.37 Å, comparable with those in the structures of Sc_2CrC_3 (3.19$-$3.45 Å)[1e] and $Sc_5Re_2C_7$ (3.21$-$3.50 Å).[47] Considering the average Sc$-$Sc distance of 3.28 Å in hexagonally close-packed scandium,[48] the shorter Sc$-$Sc contacts in Sc_3FeC_4 are indicative of bonding Sc$-$Sc interactions.

The C_2 pairs bond side-on to the Sc(1) atoms at a Sc(1)$-$C distance of 2.38 Å, while both side-on and end-on coordination to the Sc(2) atoms is observed at Sc(2)$-$C distances of 2.36 Å. Quite similar Sc$-$C distances occur in the structures of Sc_3C_4[49] or $ScCrC_2$.[2a] In view of the sum of the covalent radii of 2.21 Å,[46] we can assume significant Sc$-$C bonding.

Topological Analysis of the Charge Density Distribution in Sc_3FeC_4 and Sc_3CoC_4. As outlined above, the chemical bonding in the Sc_3TC_4 (T = Fe, Co) carbides can be rationalized by simple electron counting, assuming complete charge transfer of all valence electrons of the scandium atoms to the $[TC_4]$ moieties. Such an ionic picture is, however, in conflict with the structural parameters, suggesting weak but noticeable covalent Sc$-$C bonding. Accordingly, the descriptions Sc_3FeC_4 (**1**) and Sc_3CoC_4 (**2**) in terms of one-dimensionally extended $[TC_4]_n^{9n-}$ polyanions which are charge-balanced by Sc^{3+} counterions are insufficient to account for the complex bonding scenario displayed by these ternary carbides. To gain deeper insight into the electronic structure of these organometallic polyanions and the nature of their interaction with the surrounding scandium matrix, we performed topological analyses of the electron density distribution obtained by high-resolution X-ray diffraction studies and DFT band structure calculations. In the following, we will outline that this combined experimental and theoretical approach allows us to surpass the simple ionic picture drawn by the earlier extended Hückel (EH) calculations.[17−21]

As a result, clear evidence is found that the organometallic $[TC_4]_n^{9n-}$ polyanions are not simply embedded in a matrix of Sc^{3+} ions but also display discrete Sc$-$C bonds of noticeable covalent character. This observation supports the results of Simon et al., who concluded that partially covalent RE$-$C bonding might also occur in rare earth carbides such as $Y_2C_2I_2$.[50]

In the first step of our topological analyses, we analyzed the character of the short T$-$C bonds (Fe$-$C = 2.1074(6) and Co$-$C = 2.0886(4) Å; Table 1) in **1** and **2**. The T$-$C bond paths are close to linear (Figure 6, below) and display pronounced bond critical points (BCPs) which clearly differ in magnitude ($\rho(\mathbf{r}_c)$ = 0.590 and 0.581 e·Å^{-3}) from the corresponding ring critical points (RCPs) inside the T_2C_4 metallacycles (0.139 and 0.138 e·Å^{-3}) for **1** and **2**, respectively. We note the excellent agreement of these experimental values with those obtained by DFT calculations (Table 1). The positive sign of the Laplacian at the BCP of both T$-$C bonds suggests a significant polarity of the T$-$C bonds. This is in agreement with the atomic charges found for the transition metal cation (Q_T = +0.50 and +0.27) and the carbon atom, displaying pronounced carbanionic character (Q_C = −0.99 and −1.06) for **1** and **2**, respectively (Table 2).[51]

The nature of the Sc$-$C bonds, however, clearly differs from that of the T$-$C bonds (Figure 3). Two different Sc$-$C bonding modes are signaled by the presence of different Sc$-$C bond path topologies. Covalent side-on complexation of the Sc(2) atoms by the C_2 unit is supported by the observation of two clearly separated, curved Sc$-$C bond paths. Such bond path topology reflects the classical bonding scenario shown by early transition metal$-$olefin complexes, favoring a metallacyclopropane bonding mode.[52] We assume that the $\pi^*(C{=}C){\leftarrow}Sc$ back-donation component can be safely neglected in the case of the highly Lewis-acidic Sc atoms in **1** and **2**, in clear contrast to

(46) Emsley, J. *The Elements*; Oxford University Press: Oxford, U.K., 1999.
(47) Pöttgen, R.; Jeitschko, W. *Z. Naturforsch.* **1992**, *47b*, 358−364.
(48) Donohue, J. *The Structures of the Elements*; Wiley: New York, 1974.
(49) Pöttgen, R.; Jeitschko, W. *Inorg. Chem.* **1991**, *30*, 427−431.

(50) Ahn, K.; Kremer, R. K.; Simon, A.; Marshall, W. G.; Puschnig, P.; Ambrosch-Draxl, C. *J. Phys. Condens. Matter* **2005**, *17*, S3121−S3130. Partially covalent RE$-$C bonding has been also suggested in a theoretical charge density study on $Y[AlR_3]_3$ (R = Me, Et), another class of compounds which were earlier described as purely ionic compounds: Klimpel, G. M.; Anwander, R.; Tafipolsky, M.; Scherer, W. *Organometallics* **2001**, *20*, 3983−3992.
(51) We note that the transition metal-to-carbon bonds appear less polarized$-$relative to the AIM charges$-$when charges are derived from the monopole parameter (P_v) of the multipole model (Q_T = +0.02/−0.07 and Q_C = −0.55/−0.42 for **1** and **2**, respectively) using the approach suggested by Coppens et al. (Coppens, P.; Guru Row, T. N.; Leung, P.; Stevens, E. D.; Becker, P. J.; Yang, Y. W. *Acta Crystallogr.* **1979**, *A35*, 63−72). However, it has been shown by Volkov et al.[35] that net atomic charges derived from monopole parameters and those of AIM analyses can differ significantly and thus are not directly comparable with each other. For a comparison of monopole charges, AIM charges, and charges based on a natural population analysis (NPA) with those calculated within the generalized atomic polar tensor (GAPT) formalism, see also: Tafipolsky, M.; Scherer, W.; Öfele, K.; Artus, G.; Pedersen, B.; Herrmann, W. A.; McGrady, G. S. *J. Am. Chem. Soc.* **2002**, *124*, 5865−5880.

Table 1. Analysis of Bond and Ring Critical Points in (a) Sc_3FeC_4 and (b) $Sc_3CoC_4{}^a$

unit	method	distance^b	$\rho(\mathbf{r}_c)$	$\nabla^2\rho(\mathbf{r}_c)$	ellipticity ϵ	$H(\mathbf{r}_c)$	$G(\mathbf{r}_c)/\rho(\mathbf{r}_c)$
			(a) Sc_3FeC_4				
Fe−C	experiment	2.1074(6)	0.590	5.3	0.01	−0.209	0.987
	theory	2.1074	0.553	4.5	0.11	−0.194	0.923
Sc(1)−C	experiment	2.3780(4)	0.282	3.9	2.75	−0.005	1.004
	theory	2.3780	0.301	4.2	2.60	−0.010	1.018
Sc(2)−C	experiment	2.3631(6)	0.353	3.6	1.41	−0.056	0.885
	theory	2.3631	0.332	3.5	0.59	−0.046	0.880
C−C	experiment	1.4498(11)	1.750	−9.8	0.27	−2.272	0.902
	theory	1.4498	1.765	−14.8	0.00	−2.421	0.776
[Sc(2)C$_2$] RCP	experiment		0.335	4.0		−0.035	0.952
	theory		0.308	4.6		−0.005	1.060
[Fe$_2$C$_4$] RCP	experiment		0.139	0.8		−0.011	0.488
	theory		0.052	0.4		0.005	0.515
			(b) Sc_3CoC_4				
Co−C	experiment	2.0886(4)	0.581	5.4	0.17	−0.196	1.002
	theory	2.0886	0.572	3.8	0.08	−0.226	0.869
Sc(1)−C	experiment	2.3761(3)	0.299	3.4	10.71	−0.027	0.895
	theory	2.3761	0.308	3.7	2.36	−0.025	0.940
Sc(2)−C	experiment	2.3576(4)	0.337	4.0	2.35	−0.037	0.949
	theory	2.3576	0.333	3.5	0.59	−0.046	0.883
C−C	experiment	1.4539(8)	1.813	−12.0	0.09	−2.449	0.881
	theory	1.4539	1.769	−15.0	0.00	−2.433	0.773
[Sc(2)C$_2$] RCP	experiment		0.330	4.0		−0.035	0.957
	theory		0.310	4.5		−0.006	1.061
[Co$_2$C$_4$] RCP	experiment		0.138	0.9		−0.027	0.895
	theory		0.126	1.3		0.004	0.676

^{a} $\rho(\mathbf{r}_c)$ is given in e·Å^{-3}, $\nabla^2r(\mathbf{r}_c)$ in e·Å^{-5}, $H(\mathbf{r}_c)$ in hartree·Å^{-3}, and $G(\mathbf{r}_c)/(\rho(\mathbf{r}_c))$ in hartree·e^{-1}; all distances in Å. ^{b} Experimental fractional coordinates and lattice parameters were adopted and not further optimized during the band structure calculations.

Table 2. Integrated Experimental Atomic Charges (Q) of the Atomic Basins of the Crystallographically Independent Atoms in Sc_3FeC_4 and Sc_3CoC_4 (Theoretical Values Are Specified for Comparison in Square Brackets)

atomic charge	**1** (T = Fe)	**2** (T = Co)
Q_T	0.503 [0.15]	0.272 [0.07]
$Q_{Sc(1)}$	1.472 [1.60]	1.331 [1.61]
$Q_{Sc(2)}$	1.012 [1.61]	1.346 [1.62]
Q_C	−0.990 [−1.31]	−1.055 [−1.29]

the Dewar−Chatt−Duncanson (DCD)[53] bonding scenario displayed by late transition metal−olefin complexes. Pronounced $\sigma(Sc(2)-C)$ bonding is also evident from the polarization of the carbon atoms, which displays three pronounced valence shell charge concentrations (CCs) in the [T,C,Sc(2)] plane. We note that the three valence shell CCs are arranged in a trigonal planar fashion, thus suggesting a formally sp^2-hybridized carbon atom. The bonding valence shell CC(1) and CC(2) constitute integral parts of the T−C and C≡C bonds, respectively. The valence shell CC(3), however, formally represents a lone pair of carbanionic character which is prone to donate charge mainly to the Lewis-acidic Sc(2) atom and, to a lesser extent, to the Sc(1) atoms. Hence, $\sigma(Sc(2)-C)$ bonding is assisted via this directed electron delocalization process.[54]

In the case of the Sc(1)C$_2$ units, however, we identify a completely different bonding situation. Instead of two spatially separated Sc−C bond paths, we observe a single gradient path connecting the Sc(1) atom and the BCP of the C$_2$ fragment

(Figure 3). Hence, the Sc(1)C$_2$ ring and the two Sc−C BCPs have merged into a single BCP (Figure 3). Such T-type bond path topology is characteristic for olefin or acetylene transition metal complexes showing rather weak electrostatic $\sigma(C≡C) \rightarrow T$ interactions. As a result, the two crystallographically independent Sc atoms in the asymmetric units of **1** and **2** can clearly be distinguished on the basis of their (partially covalent/electrostatic) ScC$_2$ bonding characteristics. However, in both cases, Sc−C bonding is weak relative to the pronounced covalent T−C bonds in the TC$_4$ units.

The large differences in Sc−C relative to T−C bonding become even better resolved when both *electrostatic* and *energetic* aspects are considered. As a suitable method, Cremer and Kraka[55] proposed analyses of the electronic kinetic energy density, $G(\mathbf{r})$, and the potential energy density, $V(\mathbf{r})$, at the BCP, since the magnitudes of both are related to the Laplacian by an equation derived by Bader,[56,57] viz. $2G(\mathbf{r}) + V(\mathbf{r}) = \hbar^2/4m\nabla^2\rho(\mathbf{r})$. Hence, a negative value of the Laplacian indicates that the potential energy density dominates the electronic kinetic energy density at the BCPs ($|V(\mathbf{r})|/G(\mathbf{r}) > 2$).[58] However, according to a less strict criterion proposed by Cremer and Kraka, covalent bonds are already signaled by a negative value of the total energy density, $H(\mathbf{r}) = G(\mathbf{r}) + V(\mathbf{r})$.[55] In fact, the total energy density $H(\mathbf{r})$ at the BCPs becomes clearly *negative* and thus supports covalent bonding for T−C (−0.209 and −0.196 hartree·Å^{-3}), respectively, while being *insignificantly*

(52) (a) Macchi, P.; Proserpio, D. M.; Sironi, A. *J. Am. Chem. Soc.* **1998**, *120*, 1447−1455. (b) Scherer, W.; Eickerling, G.; Shorokhov, D.; Gullo, E.; McGrady, G. S.; Sirsch, P. *New J. Chem.* **2006**, *30*, 309−312. (c) Hertwig, R. H.; Koch, W.; Schröder, D.; Schwarz, H.; Hrušák, J.; Schwertfeger, P. *J. Phys. Chem.* **1996**, *100*, 12253−12260. (d) Frenking, G.; Fröhlich, N. *Chem. Rev.* **2000**, *100*, 717−774.
(53) (a) Dewar, M. J. S. *Bull. Soc. Chim. Fr.* **1951**, *18*, C71−C79. (b) Chatt, J.; Duncanson, L. A. *J. Chem. Soc.* **1953**, 2939−2947.
(54) Theoretical charge density studies of the highly Lewis-acidic [(η^2-C$_2$H$_4$)-TiCl$_2$]$^+$ cation show a similar charge donation interaction between the Lewis-acidic metal center and the corresponding valence shell CC at the sp^2-hybridized carbon atom; see ref 63a.

(55) (a) Cremer, D.; Kraka, E. *Angew. Chem., Int. Ed. Engl.* **1984**, *23*, 627−628. (b) Cremer, D.; Kraka, E. *Croat. Chem. Acta* **1984**, *57*, 1259−1281.
(56) Bader, R. F. W. *J. Chem. Phys.* **1980**, *73*, 2871−2883.
(57) While energy densities can easily be derived from theoretical electron densities obtained from quantum-chemical calculations, there is no straightforward procedure for evaluating experimental energy densities. In our experimental studies, we have used the approach developed by Abramov to derive $G(\mathbf{r})$ from the total charge density; see also: Abramov, Yu. A. *Acta Crystallogr.* **1997**, A*53*, 264−272. Alternatively, $G(\mathbf{r})$ and $V(\mathbf{r})$ might be derived by constraining the theoretical wave function of a model system to the experimental structure factors of the real system; see: (a) Jayatilaka, D.; Grimwood, D. J. *Acta Crystallogr. Sect. A* **2001**, *57*, 76−86. (b) Jayatilaka, D.; Grimwood, D. J. *Acta Crystallogr. Sect. A* **2004**, *60*, 111−119.
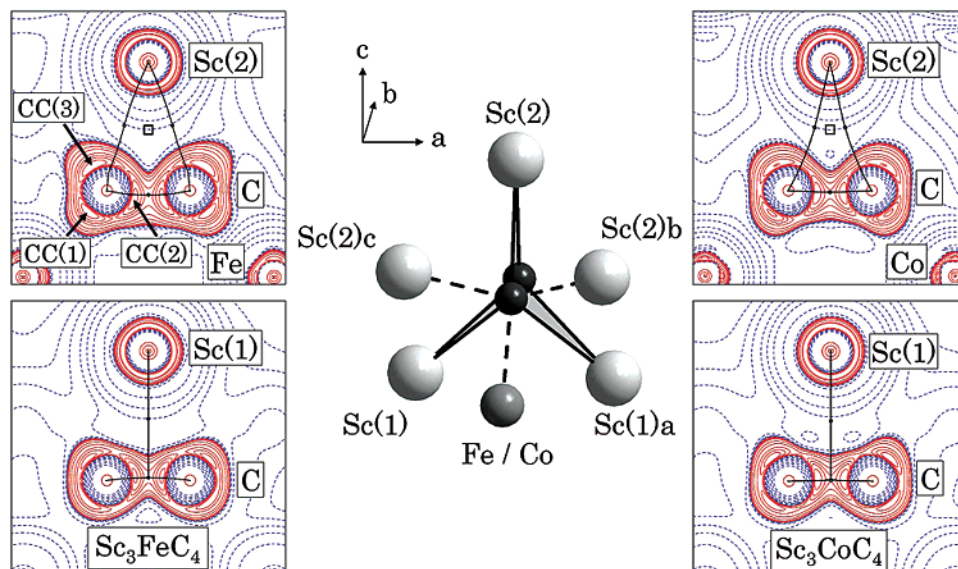
Figure 3. Octahedral coordination sphere of the C atoms in **1** and **2** and experimental $L(\mathbf{r}) = -\nabla^2\rho(\mathbf{r})$ maps showing the T-type bond path of the Sc(1)C$_2$ fragment and the separated Sc(2)−C bond paths in the Sc(2)C$_2$ plane, respectively. Contour levels are drawn at 0.001, ±2.0 × 10^n, ±4.0 × 10^n, and ±8.0 × 10^n e·Å^{-5}, where n = 0, ±3, ±2, ±1; extra levels at 11.5, 15.0, 1200, and 1500 e·Å^{-5}. Positive and negative values are marked by solid and dashed lines, respectively. Bond critical points (BCPs) and ring critical points (RCPs) are marked by closed circles and squares, respectively. The bond paths of the Sc(1)C$_2$ and Sc(2)C$_2$ moieties are marked by solid lines; symmetry-related atomic coordinates are as follow: (a) 1+x, y, z; (b) 0.5+x, 0.5−y, 0.5−z; and (c) −0.5+x, 0.5−y, 0.5−z. The positions of the charge concentrations CC1, CC2, and CC3 in the valence shell of the carbon atoms of **1** are indicated by arrows.

negative in the case of the Sc−C bonds (−0.005 to −0.056 hartree·Å^{-3}) of **1** and **2**. At this stage, the bonding differences between carbon and the Sc(1)/Sc(2) atoms are not revealed by energetic arguments based on $H(\mathbf{r})$.[59] However, $G(\mathbf{r})/\rho(\mathbf{r})$ ratios significantly smaller than unity (0.89/0.95 hartree·e^{-1} for **1** and **2**, respectively) support the weak but noticeable character of the Sc(2)−C bonds in **1** and **2**.[60] This result is in line with the slightly higher charge density accumulation found at the Sc(2)−C BCPs ($\rho(\mathbf{r}_c)$ = 0.353/0.337 e·Å^{-3} in **1** and **2**, respectively) relative to the corresponding Sc(1)−C BCPs (Table 1).

At this stage of our analysis, we can already conclude that the various and noticeable Sc−C interactions should lead to a complex charge-ordering pattern in Sc$_3$TC$_4$. Hence, the earlier ionic model, assuming the presence of [TC$_4$]$^{9-}$ polyanions, needs to be developed further. In the second step of our analysis, we have therefore performed a more quantitative analysis of the charge ordering in Sc$_3$TC$_4$, by calculating experimental atomic charges. These were obtained from the integrated charge densities of the individual atomic basins of the Fe/Co, Sc(1), Sc(2), and C atoms (Table 2). The carbon atoms in **1** and **2** display a negative charge of about one electron per atomic basin (Q_C = −0.99/−1.06, respectively), while the transition metal atoms are weakly oxidized and carry a modest charge of Q_{Fe} =

+0.50 and Q_{Co} = +0.27. Based on the experimental atomic charges and our band structure calculations (see below), the electronic situation of the [TC$_4$] moieties might thus be modeled by square planar [TC$_4$]$^{(4-x)-}$ moieties, where x represents the degree of oxidation or magnitude of the positive charge of the transition metal center ($x = Q_T$). The total charge of the [TC$_4$]$^{(4-x)-}$ units is then counter balanced by the three Sc cations of the formula unit. Thus, the [FeC$_4$]$^{(4-x)-}$ units might be interpreted as the first example of an organometallic Fe(d^8) tetraalkylidene species if we neglect the partial oxidation of the iron center in Sc$_3$FeC$_4$. We note that the existence of square planar organometallic [FeR$_4$]$^{4-}$ (R = alkyl, phenyl) complexes has been claimed for decades in the chemical literature. However, the celebrated example of such an Fe(d^8) species, [Li-(Et$_2$O)]$_4$[FePh$_4$] (**6**),[61] turned out to be most likely a case of a mistaken identity.[62]

Despite the subtle charge balance accomplished by the various Sc−C interactions in the planar [TC$_4$]$^{(4-x)-}$ moieties, a pronounced carbanionic character of the carbon atoms is still evident. As a consequence, significant weakening of the C=C double bonds due to occupation of antibonding π^*(C−C) orbitals is observed. Indeed, the C−C bond distances of 1.4498(11) and 1.4539(8) Å in **1** and **2**, respectively, fall in a narrow range marked by transition metal−ethyl complexes with shortened C−C single bond distances (e.g., 1.5126(12) Å in

(58) We note that the $|V(\mathbf{r})|/G(\mathbf{r})$ ratio has recently been used as an alternative classification index for the covalency of bonds. According to Espinosa et al., values larger than 2 (which correspond to negative $H(\mathbf{r})$ values) are indicative of covalent bonds; see: Espinosa, E.; Alkorta, I.; Elguero, J.; Molins, E. *J. Chem. Phys.* **2002**, *117*, 5529−5542.

(59) One of the reviewers pointed out that the Sc(1)−C and Sc(2)−C bonds can be distinguished by scaling the total energy density on the values of the electron density, $H(\mathbf{r}_c)\rho(\mathbf{r}_c)$, at the BCPs. Indeed, the Sc(2)−C BCP in **1** displays a scaled total energy density ($H(\mathbf{r}_c)\rho(\mathbf{r}_c)$ = −0.16 hartree/e) which is in the range of the more covalent Fe−C bond (−0.35 hartree/e) and at variance from the value found for the more electrostatic Sc(1)−C bond (−0.02 hartree/e). However, in the case of the cobalt compound **2**, the $H(\mathbf{r}_c)\rho(\mathbf{r}_c)$ differences at the Sc(2)−C and Sc(1)−C BCPs are less pronounced: −0.11 and −0.09 hartree/e, respectively.

(60) Macchi, P.; Proserpio, D. M.; Sironi, A. *J. Am. Chem. Soc.* **1998**, *120*, 13429−13435.

(61) Bazhenova, T. A.; Lobkovskaya, R. M.; Shibaeva, R. P.; Shilova, A. K.; Gruselle, M.; Leny, G.; Deschamps, E. *J. Organomet. Chem.* **1983**, *244*, 375−382.

(62) As demonstrated by Girolami et al. in 1998, not an Fe(d^8) complex but the Fe(d^6) dihydride [Li(Et$_2$O)]$_4$[FeH$_2$Ph$_4$] (**7**) was originally synthesized by Shilov et al. in 1983. The ferrate dihydride **7** displays, like **1**, a square planar coordinated Fe moiety, but the isoelectronic [Li(tmeda)]$_2$[Co(CH$_2$-SiMe$_3$)$_4$] highlights the fact that usually tetrahedral structures are observed for homoleptic [T(d^6)C$_4$]$^{2-}$ complexes. Indeed, the recent example of a homoleptic tetra-alkyl-ate iron complex, [(Me$_4$Fe)(MeLi)][Li(OEt$_2$)]$_2$, again displays a tetrahedrally coordinated [Fe(d^6)C$_4$]$^{2-}$ complex center which clearly differs from the scenario found in the polymeric square planar [FeC$_4$]$^{(4-x)-}$ units of Sc$_3$FeC$_4$. See: (a) Jefferis, J. M.; Girolami, G. S. *Organometallics* **1998**, *17*, 3630−3632. (b) Jefferis, J. M.; Girolami, G. S. *Organometallics* **1999**, *18*, 3768−3768.
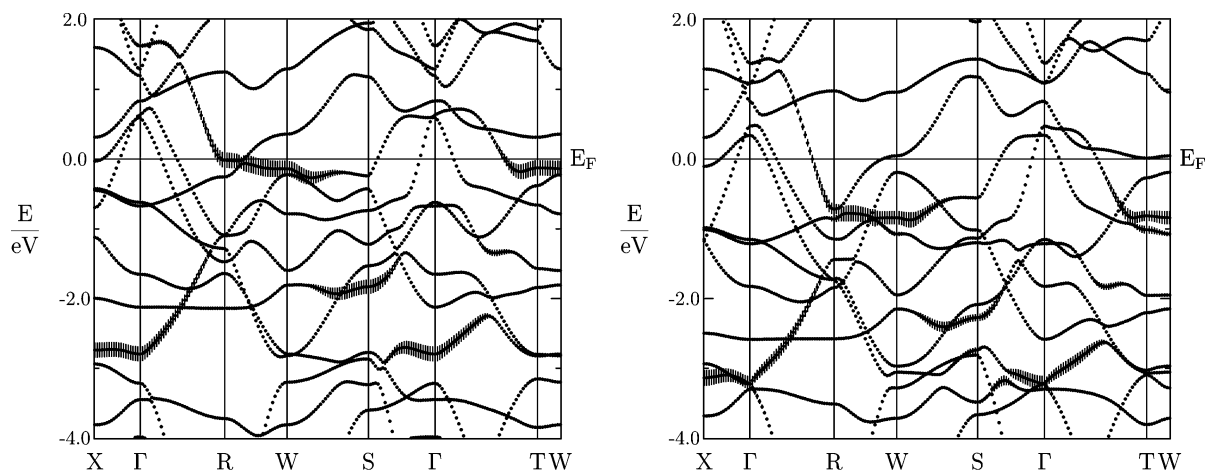
Figure 4. Electronic bands of the ternary carbides **1** (left) and **2** (right) along selected symmetry lines within the first Brillouin zone of the *I*-centered orthorhombic unit cell. The widths of the bars given for each band indicate the contribution due to the $3d_{3z^2-r^2}$ orbital of the Fe or Co atoms, respectively. For a definition of the Brillouin zone and other relevant orbital contributions to the individual electronic bands, see the Supporting Information.

$(C_2H_5)TiCl_3(dmpe)$ (**3**), dmpe = $Me_2PCH_2CH_2PMe_2)^{63}$and transition metal−olefin complexes with weakened C=C double bonds (e.g., 1.4189(6) Å in $\eta^2(C_2H_4)Ni(dbpe)$ (**4**), dbpe = Bu^t_2-$PCH_2CH_2PBu^t_2)$.[64] However, the C−C bond distances clearly differ from those of transition metal−acetylene complexes displaying C−C triple bonds (e.g., 1.209(1) Å in $[Ag(C_2H_2)$-$Al(OCCH_3(CF_3)_2)_4]$ (**5**)).[65] Note that the C−C bond distances in all benchmark systems **1**−**5** are directly comparable since they are based on multipolar refinements employing high-resolution X-ray data. Therefore, these distance parameters can be considered as being virtually deconvoluted from thermal smearing effects. We further note that the C−C bonds in **1** and **2** are characterized by relatively weakly pronounced C−C BCPs ($\rho(\mathbf{r})$ = 1.750/1.813 e·Å^{-3} and $\nabla^2\rho(\mathbf{r})$ = −9.8/−12.0 e·Å^{-5}) in **1** and **2**, respectively. These values compare well with those of our benchmark system **3**, displaying a C−C single bond with partial double bond character (for **3**, $\rho(\mathbf{r})$ = 1.77(3) e·Å^{-3} and $\nabla^2\rho(\mathbf{r})$ = −12.06(7) e·Å^{-5}), but clearly deviate from those of our benchmarks for olefin−transition metal or acetylene−transition metal complexes (for **4**, $\rho(\mathbf{r})$ = 2.107(9) e·Å^{-3} and $\nabla^2\rho(\mathbf{r})$ = −20.88(3) e·Å^{-5}; for **5**, $\rho(\mathbf{r})$= 2.80 e·Å^{-3} and $\nabla^2\rho$-$(\mathbf{r})$ = −29.6 e·Å^{-5}). Accordingly, the bonding situation in the C_2 units of **1** and **2** might be best classified by C−C bonds displaying a reduced double-bonding character.[66]

It is remarkable that the cobalt analogue, which shows a more pronounced charge accumulation/contraction at the BCP relative to **1**, displays the larger C−C separation. This result is in agreement with our assumption that electrons transferred to the carbanionic C_2 units occupy C−C antibonding levels and thus cause the stretching of the C−C bonds. This subtle trend is also in line with our DFT calculations (Table 1). Hence, on the basis of the structural data and the topological analysis of the charge density alone, the electronic structures of Sc_3FeC_4 and Sc_3CoC_4 appear nearly indistinguishable. However, we will outline in the following that we are able to identify the subtle changes in the electron density distribution when we move from Sc_3FeC_4 to the isotypic cobalt analogue, a step which changes the total electron balance just by a single electron.

Table 3. Comparison of the d-Orbital Population (*P*) Derived from the Experimental Multipole Populations of **1** and **2**

P	D_{4h}	Fe in **1**	Co in **2**
x^2-y^2	b_{1g}	1.55(9)	1.47(7)
$3z^2-r^2$	a_{1g}	1.60(9)	1.80(6)
xz,yz	e_g	2 × 1.41(4)	2 × 1.84(3)
xy	b_{2g}	2.02(9)	2.12(7)
total (P_v)		7.98(10)	9.07(6)

Atomic d-Electron Population in 1 and 2. We demonstrated above that the ternary carbides **1** and **2** represent benchmark systems of isotypic compounds displaying charge density distributions that do not differ significantly. Indeed, from the viewpoint of X-ray crystallography, the differentiation between **1** and **2** represents a rather extreme case of a coloring problem since the scattering factors of iron and cobalt are very similar, as implied by the ratio of the electron count Z(Fe)/Z(Co) = 26/27, which is close to unity. Furthermore, the suitability factor,[67] representing a measure for the suitability of a crystal for an experimental charge density study, is 0.07 in the cases of **1** and **2**. This value is much smaller than the typical values (3−5) displayed by organic compounds and suggests there would be severe experimental complications in solving the coloring problem of **1** and **2** by X-ray methods, since the core-

(63) (a) Scherer, W.; Sirsch, P.; Shorokhov, D.; Tafipolsky, M.; McGrady, G. S.; Gullo, E. *Chem. Eur. J.* **2003**, *9*, 6057−6070. (b) Scherer, W.; McGrady, G. S. *Angew. Chem., Int. Ed.* **2004**, *43*, 1782−1806.

(64) Scherer, W.; Eickerling, G.; Shorokhov, D.; Gullo, E.; McGrady, G. S.; Sirsch, P. *New J. Chem.* **2006**, *30*, 309−312.

(65) Reisinger, A.; Trapp, N.; Krossing, I. Altmannshofer, S.; Herz, V.; Presnitz, M.; Scherer, W. Manuscript in preparation.

(66) A pioneering study by Simon and co-workers (Miller, G. J.; Burdett, J. K.; Schwarz, C.; Simon, A. *Inorg. Chem.* **1986**, *25*, 4437−4444) concluded that the measured C-C bond length in solid-state rare earth or alkaline earth metal dicarbides can be directly correlated with the effective negative charge of the C_2 units and hence to its formal C−C bond order. According to this study, the C−C bond distances of **1** and **2** would fall in the range allocated for $(C_2)^{6-}$ anions displaying a C−C bond order of 1. However, as demonstrated by Halet and co-workers (Frapper, G.; Halet, J.-F. *Organometallics* **1995**, *14*, 5044−5053), this simple bonding picture only holds for purely ionic dicarbides. In this respect, the presence of pronounced covalent bonding in **1** and **2** rules out a simple ionic description in terms of isolated $(C_2)^{n-}$ anions. As an alternative, we find that Halet's bonding picture, developed for dicarbides encapsulated in metal clusters, appears more appropriate to account for the C−C bonding situation in **1** and **2**. In this model, the C_2 units are formally considered as dianionic species—in agreement with the octet rule and the observed AIM charges of **1** and **2**, which act as eight-electron donors. As a result, the variation of the C−C distances depends basically on the electronic effects coming from the metallic environment. Indeed, remarkably long C−C distances can also be found for C_2 units encapsulated in metal clusters: e.g., $Co_6(C_2)(CO)_{18}$ (prismatic Co_6 coordination; C−C = 1.426(9) Å) and $[Co_9(C_2)(CO)_{19}]^{2-}$ (tricapped Co_9 prism; C−C = 1.39(2) Å). See: (a) Geiser, U.; Kini, A. M. *Acta Crystallogr.* **1993**, *C49*, 1322−1324. (b) Martinengo, S.; Noziglia, L.; Fumagalli, A.; Albano, V. G.; Braga, D.; Grepioni, F. *J. Chem. Soc., Dalton Trans.* **1998**, 2493−2496.

(67) Stevens, E. D.; Coppens, P. *Acta Crystallogr.* **1976**, *A32*, 915−917.
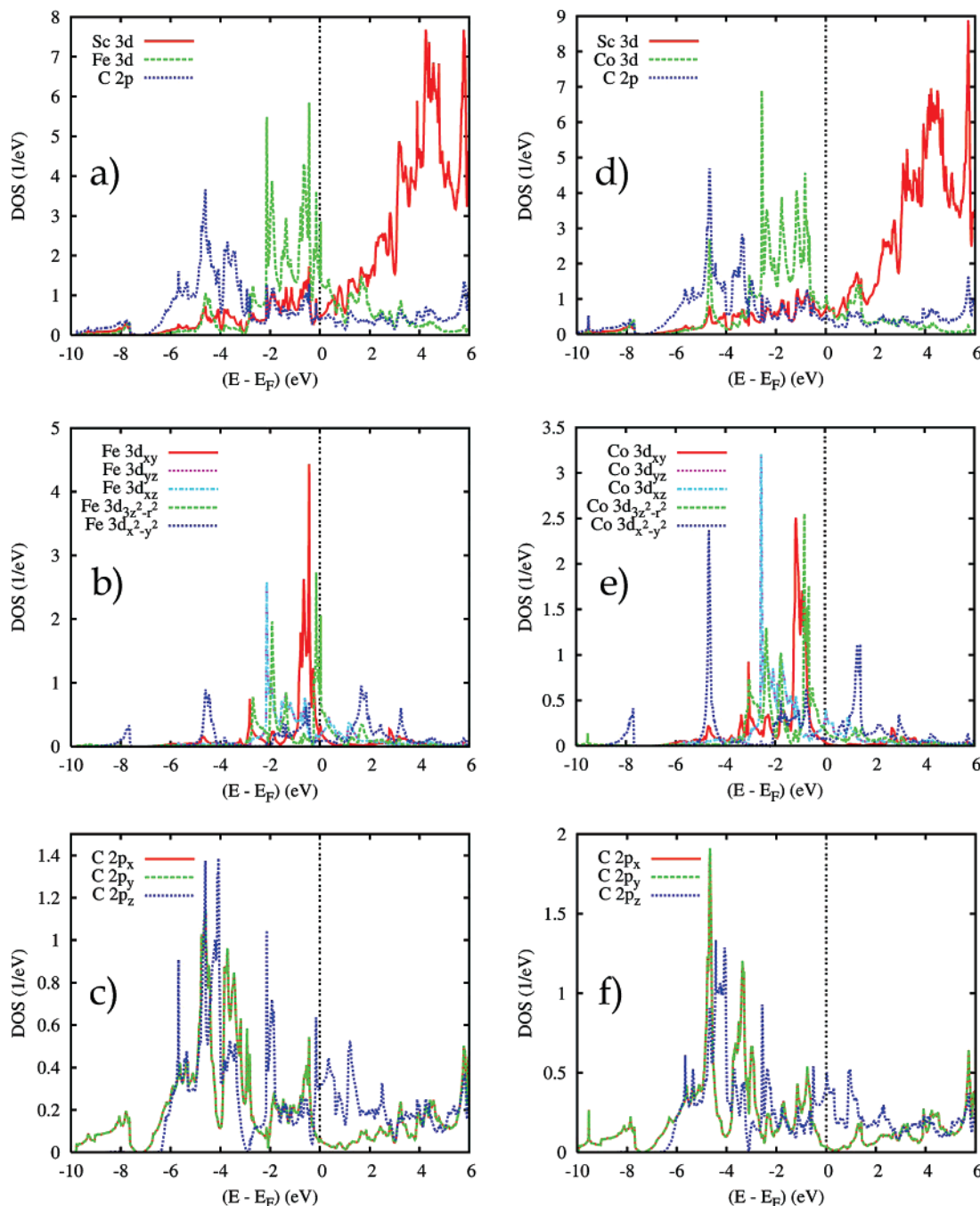
Figure 5. (a−f) Site- and state-projected partial densities of states (DOS) for both ternary carbides **1** (left) and **2** (right) in the energy range between −10 and 6 eV. The position of the Fermi level (E_F) is specified by a dashed line.

scattering intensity per unit volume is rather high. However, we will outline in the following that the *local* charge density distribution around the transition metal atoms differs significantly and allows distinction of the iron and cobalt compounds on the basis of precise high-resolution X-ray data alone.

Analysis of the d-orbital populations derived from the experimental multipole models[68] of **1** and **2** shows that the above-mentioned coloring problem can be solved by means of experimental X-ray data. If we consider only the first coordination sphere of the transition metals in **1** and **2**, namely the [TC_4] units, the symmetry of the crystal field can be specified by local

D_{4h} symmetry (Figure 1).[69] Therefore, the precise crystallographic site symmetry (*mmm* or D_{2h}) at the iron and cobalt sites can safely be approximated by D_{4h} symmetry.

In the next step of our analysis, we will focus on the electronic structure of the iron compound first. In the framework of the electrostatic crystal field theory, which ignores any σ and π interactions between the iron atom and the C_2 units, simple symmetry considerations suggest a standard $(b_{2g})^2 (e_g)^4 (a_{1g})^2$ ordering of the d-orbitals at the iron atom (Table 3), displaying a formal d^8 electron configuration. However, we have demon-

(68) Holladay, A.; Leung, P.; Coppens, P. *Acta Crystallogr.* **1983**, *A39*, 377−387.

(69) Indeed, analysis of the d-orbital population derived from the experimental multipolar model shows that the cross terms in both carbides are not significantly populated. For **1**, $P(3z^2−r^2/xy) = −0.19(20)$ and $P(xz/yz) = 0.12(21)$; for **2**, $P(3z^2−r^2/xy) = −0.11(14)$ and $P(xz/yz) = 0.10(15)$.
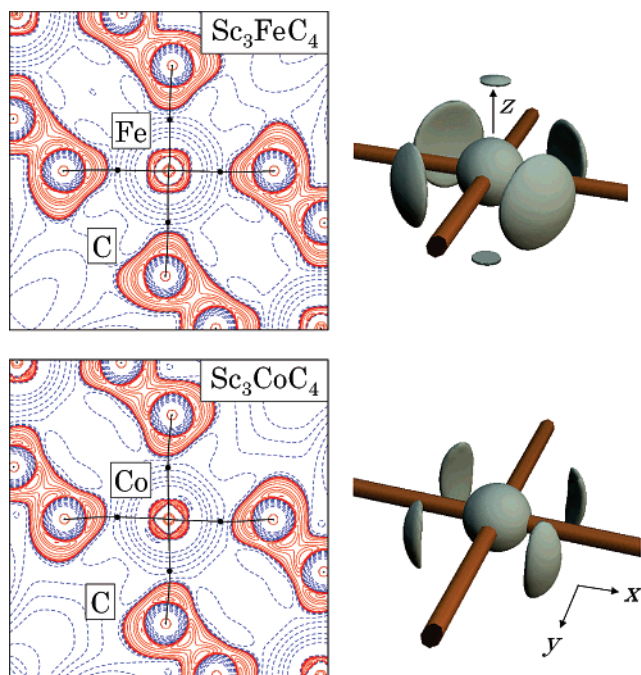
Figure 6. (Left) $L(\mathbf{r})$ contour maps of the experimental electron density of **1** (top) and **2** (bottom) in the b,c plane. For a specification of the contour levels, see Figure 3. (Right) Envelope map of the negative Laplacian of the experimental charge density of **1** and **2**; $L(\mathbf{r}) = 800$ and 1600 e·Å^{-5}, respectively. Note the additional charge concentrations above and below the [FeC$_4$] plane in the case of **1**.

strated in the previous section that the atomic charge of $Q_{Fe} = +0.5$ suggests a partial oxidation of the iron atom. Indeed, band structure calculations (see below) show that the a_{1g} bands which cross the Fermi level are slightly depopulated and constitute the conduction band in **1**.

Analysis of the d-orbital population of the central iron atom derived from experimental multipole population parameters (Table 3) shows a significant depopulation of the crystal-field-stabilized e_g (d_{xz},d_{yz}) orbitals ($P = 1.41(4)$) relative to a hypothetical high-spin spherical iron ion with a valence count of $P_v = 7.98(10)$, which displays an averaged d-orbital population of $P = 1.60$. At the same time, the crystal-field-destabilized $d_{x^2-y^2}$-orbital is clearly occupied ($P = 1.55(9)$). These results show that a simple electrostatic crystal field description of the electronic structure of Sc$_3$FeC$_4$ is inappropriate since pronounced covalent σ(Fe−C) bonding is at work. This conclusion is supported by analyzing the electronic band structure of **1**.

Electronic Band Structures of 1 and 2. Calculated bands and partial, i.e., site- and state-projected, densities of states (DOS) for both ternary carbides **1** and **2** in the energy range between −10 and 6 eV are shown in Figures 4 and 5. In assigning the orbitals, we used a rotated reference frame with the local z-axis perpendicular to the Fe/Co−C planes and the x- and y-axis pointing along the Fe/Co−C bonds.

Concentrating on the iron compound first, we observe in the band structure a somewhat reduced dispersion along the lines $X−\Gamma$ and $T−W$, which reflects the low dimensionality of the crystal structure due to the formation of the Fe−C ribbons. However, the still finite dispersion of some bands along the former lines points to a more complex bonding pattern.

In the partial DOS, four energy regions can be distinguished. In the interval from −10 to −7 eV, mainly C(p$_{x,y}$) states are

observed, with an admixture of Fe(3d$_{x^2-y^2}$) states at about −8 eV. Carbon states also dominate the interval from −7 to about −3 eV. However, there are again admixtures from the other atoms, mainly from Fe(3d$_{x^2-y^2}$) states of b_{1g} symmetry.[70] The latter contributions are due to the strong σ-type bonding between these orbitals, and the in-plane carbon p-orbitals and are indicated by a peak at about −4.5 eV. The corresponding antibonding peaks are clearly observed at 1.8 and 3.2 eV (Figure 5b).

The interval from −3 to about 1 eV is characterized mostly by Fe(3d) states, and at energies above 1 eV the main contributions of the Sc(3d) states set in. Worth mentioning is the strong Fe(3d$_{xy}$) peak at about −0.6 eV. These d-orbitals of b_{2g} symmetry do not participate significantly in covalent bonding, hence their sharp structure. However, the small but distinct splitting of this peak might be reminiscent of small metal−metal bonding along the direction of the ribbons. We note, however, that such a bonding interaction is not supported by any BCP in the charge density distribution of **1** (and **2**). Hence, solely the d$_{xy}$-orbitals basically keep their nonbonding character in the D_{4h}-symmetric [FeC$_4$] units and are fully occupied ($P = 2.02(9)$) in the range of the experimental errors (Table 3).

We point also to the strong splitting of the Fe(3d$_{3z^2-r^2}$) states of a_{1g} symmetry into two sharp peaks at −1.9 eV and just below the Fermi level, which are complemented by peaks in the C(p$_z$) partial DOS and reflect, for symmetry reasons, basically nonbonding interactions between these orbitals. A sharp feature at −2.1 eV signals the presence of π-type bonding in the [FeC$_4$] units involving the carbon out-of-plane p$_z$ orbitals and the metal e_g orbitals (Fe 3d$_{xz}$ and 3d$_{yz}$). We suggest that this type of π-interaction is responsible for charge back-donation from the e_g metal orbitals into the antibonding π*(C−C) orbitals of the C$_2$ units. Such π-interaction must be oriented out-of-plane of the FeC$_4$ units. This conclusion is also supported by the topological features of the C−C bonds, which render *longer* and *weaker* despite the increasing accumulation of electron density at the corresponding BCP when we move from the iron to the more electron-rich cobalt carbide. However, since the additional electron in the cobalt compound relative to the iron carbide is rather delocalized over the extended polymeric [CoC$_4$] units, the structural and topological trends, as outlined above, are rather weak, despite being significant. Hence, analysis of the electronic bands clearly provides evidence for the presence of covalent σ- and π-bonding inside the organometallic poly-anions, in agreement with the d-orbital populations derived from the experimental multipolar model.

The major difference between the electronic structures of **1** and **2** is connected with the additional d electron present in the cobalt species **2** relative to the iron carbide **1**, causing an increase of the Fermi level. The partial DOS of **1** and **2**, depicted in Figure 5, reveal that the bands crossing the Fermi level basically display nonbonding Fe(3d$_{3z^2-r^2}$)/C(p$_z$) character in the case of the iron and antibonding Co(d$_{xz}$,d$_{yz}$)/C(2p$_z$) character in the cobalt analogue.

Our population analysis and band structure interpretation is finally supported by the topological analysis of the negative

---

(70) Note that, in the following discussion, the symmetry symbols refer to the local D_{4h} point symmetry displayed by the central iron atom inside the square planar [FeC$_4$] units.

Laplacian of the charge density $L(\mathbf{r})$, which shows pronounced charge concentrations in the domain of the fully occupied nonbonding d_{xy}-orbital of the iron and cobalt atoms of **1** and **2**, respectively (Figure 6). Hence, the presence of covalent σ-bonding inside the planar [TC$_4$] units leads to pronounced differences in the population of the $T(d_{xy})$ and $T(d_{x^2-y^2})$ orbitals, which again induce a clear in-plane polarization of the valence density of the transition metal atoms. However, despite these similarities, the polarization patterns of **1** and **2** differ significantly. In contrast to **2**, the polarization pattern of **1** shows two charge concentrations above and below the FeC$_4$ plane. This axial polarization is again a consequence of an unequal occupation of the transition metal d-orbitals (Table 3). Indeed, the ratio of $P(3d_{3z^2-r^2}/d_{xz})$ and $P(3d_{3z^2-r^2}/d_{yz})$ is larger than unity only in the iron compound, thus giving rise to an axial polarization pattern.

To conclude, the increase of the Fermi level in **2** relative to **1** is reflected in our experimental charge density picture by a change of the polarization pattern of the central transition metal in the TC$_4$ units. Hence, the filling of the antibonding bands of Co(d_{xz},d_{yz})/C($2p_z$) character in **2** finds a charge density analogue

in the vanishing of the axial polarization pattern due to a reversal of the $P(3d_{3z^2-r^2}/d_{xz})$ and $P(3d_{3z^2-r^2}/d_{yz})$ population ratio.

Supporting Information Available: Tables of crystal data, details of the structure solution and refinement, atomic coordinates, anisotropic thermal parameters and residual electron density maps, specifications of local coordinate systems employed, multipole parameters for **1** and **2**, definition of the Brillouin zone and other relevant orbital contributions to the individual electronic bands of **1** and **2**, theoretical $L(\mathbf{r})$ maps and bond paths, and ^{57}Fe Mössbauer spectra of **1** at 4.2 and 77 K (PDF); X-ray crystallographic data for **1** and **2** (CIF). This material is available free of charge via the Internet at http://pubs.acs.org.

JA068137Y